Photoionization cross sections of the ground and first excited states of the OH radical

Kedong Wang ,* Jie Liu, Haoxing Zhang, and Yufang Liu
School of Physics, Henan Normal University, Xinxiang 453007, People's Republic of China

(Received 18 February 2021; accepted 18 May 2021; published 1 June 2021)

We present a comprehensive study of photoionization of OH radicals from the ground and first excited electronic states. Cross sections and asymmetry parameters for the valence orbitals are reported for photon energies from near the threshold to 60 eV. The calculations have been performed with the *R*-matrix method. Two different continuum basis types, namely, the Gaussian and *B*-spline bases, are used to assess the quality of the description of the continuum. The results show both types of continuum bases provide a similar quality description in the near threshold resonant region, but the latter can predict more reliable photoionization observables in higher-energy regions. Our calculations are compared with available experimental and theoretical results, and the discussions are provided.

DOI: 10.1103/PhysRevA.103.063101

I. INTRODUCTION

The removal of an electron from an atom or molecule by the action of light, photoionization, is an important process in modeling and understanding aeronomy, planetary science, radiation chemistry and physics, and industrial plasma [1]. It is the primary source of ions produced in the interstellar medium and the upper atmosphere of astral bodies. Accurate and reliable photoionization data are required to interpret the chemical and physical properties and reaction pathways in these environments such as planetary atmospheres, interstellar molecular clouds, and solar nebulas [2]. Photoionization itself is a highly correlated process that provides a rigorous test for theories and computational methods, thereby supporting their further development.

The hydroxyl radical, OH, is one of the most important free radicals in the atmosphere [3], combustion oxidation [4], and in the interstellar medium [5]. As a second-row hydride, OH has served as an important benchmark for fundamental studies of electronic spectroscopy and structure. Accurate spectroscopic information has been obtained about its low-lying electronic states. For the ionization process, three experimental studies have reported the relative photoionization spectra of the hydroxyl radical in the VUV range. van Lonkhuyzen and de Lange [6] have employed techniques of ultraviolet photoelectron spectroscopy to determine the ionization potentials leading to the four low-lying ionic states. Dehmer [7] recorded spectra with a resolution of 1–3 meV for the photon energy range from 13.0 to 16.5 eV. This spectrum agrees with a later spectrum from Cutler *et al.* [8] obtained between 13.1 and 18.2 eV at a resolution of 1 meV. Recently, the absolute photoionization cross section of the OH radical has been measured. Dodson *et al.* [9] deduced the cross section from the analysis of time-resolved radical-kinetics measurements of a multireaction network in which OH is produced in the reaction of $O(^1D)$ with H_2O. The absolute cross section of OH was determined relative to that of $O(^3P)$. Their work was supported by new theoretical calculations of the OH cross section using equation-of-motion coupled-cluster Dyson orbitals and a Coulomb photoelectron wave function. Subsequently, Harper *et al.* [10] determined the absolute photoionization cross section by a different method. They produced the OH radical via H abstraction of H_2O by F atoms ($H_2O + F \rightarrow HO + HF$), and set it to an absolute cross-section scale using the known cross sections of H_2O and O. However, the resulting cross section values from Harper *et al.* [10] differ by approximately a factor 2 from the measurement of Dodson *et al.* [9], which is somewhat greater than the combined uncertainties of the measurements. This indicates that further investigations of photoionization cross section, such as theoretical calculations, are needed.

On the theoretical side, the photoionization spectra of the OH radical were reported by several groups. A study by Stephens and McKoy [11], based on the Schwinger variational method using multiplet-specific Hartree-Fock (MSHF) potentials and numerical continuum orbitals, predicted cross sections and photoelectron angular distributions for the 3σ and 1π levels of OH. However, it was pointed out that significant deviations could occur due to the correlation not being included in the approach [12]. Later Veseth and Kelly [12] reinvestigated the photoionization cross section of OH by an integral equation approach with many-body perturbation theory, taking into account single-electron excitation and molecular polarization. However, the strong interaction between the filled 3σ shell and the open 1π shell leads to problems with the convergence of the perturbation expansion and they had to use a model Hamiltonian. Finally, based on total transition probability between two electronic molecular levels determined from vibrational transition probabilities and Hönl-London factors, Riahi *et al.* [13] reported the photoionization cross sections from the ground state of OH to the first excited state. All these calculations predicted sparse spectra, and no study provided much detail near the ionization threshold.

*wangkd@htu.cn

The goal of the present work was to carry out a comprehensive study of photoinduced cross sections of OH radicals. Here we employ a multichannel, wave-function based, R-matrix approach [14], which uses the configuration interaction (CI) method to describe electronic correlation. The other purpose of this paper is to explore the advantages of using different continuum descriptions in R-matrix calculations. The performance of this method using Gaussian-type orbitals (GTOs) for continuum descriptions has recently been demonstrated in studies of photoionization of NO_2 [15], CO [16], and H_2O [17]. However, recent efforts were directed toward the extension of the UKRMOL+ code [14] to make it possible to use B-spline type orbitals (BTOs). So far only one publication [18] has presented multichannel R-matrix photoionization cross section determined using BTOs. A comparison of these two continuum basis types has been made in the present work.

This paper is organized as follows. Section II describes the computational method for the structure and the photoionization processes. Some tests of various models for the studied photoionization cross section are described in Sec. III. This is followed by a presentation of the final result and discussion in Sec. IV, and finally the conclusions in Sec. V.

II. COMPUTATIONAL DETAILS

A. Theoretical method

The photoionization cross sections in the length gauge are given by [19,20]

$$\frac{d\sigma_{if}}{dk_f} = 4\pi^2\alpha a_0{}^2\omega|d_{if}(k_f)\cdot\hat{\epsilon}|^2, \tag{1}$$

where α is the fine structure constant, a_0 is the Bohr radius, ω is the photon energy in atomic units, and ϵ is the polarization vector of the ionizing light in the molecular frame. $d_{if}(k_f)$ is the molecular frame transition dipole between the initial state, i, and a single continuum state, j, as a function of the ejected electron momentum, k_f.

If the molecular frame cannot be recovered, Eq. (1) must be orientationally averaged and in the case of a linearly polarized laser field one obtains

$$\overline{\left(\frac{d\sigma_{if}}{dk_f}\right)} = \frac{\sigma_{if}}{4\pi}[1+\beta P_2(\cos\theta)], \tag{2}$$

where β is the asymmetry parameter, σ_{if} is the partial photoionization cross section, P_2 is the second-order legendre polynomial, and θ is the electron ejection angle between the photoelectron emission direction and photon polarization direction in the case of linear polarization. In the present paper, an R-matrix calculation is used to present the bound and the continuum wave functions in Eq. (1).

In an R-matrix approach [21], the configuration space of the scattering system is divided into two spatial regions: an inner region and an outer region. The inner region radius is chosen such that all short-range interactions are contained within it. The target wave function and corresponding charge density are assumed to be completely included in this sphere, and the electron-target interaction is represented through exchange and correlation potentials. In the outer region, long-range multipolar interactions of the scattering electrons with different target states are considered by using a single center close-coupling (CC) approximation. At the interface, energy-independent solutions from the inner region are used to construct an energy-dependent R matrix.

In the inner region, both the continuum and the bound-state wave functions are given in terms of the basis functions, ψ_k^N, as

$$\Psi_f^{(-)N}(k_f) = \sum_k A_{fk}^{(-)}(k_f)\psi_k^N(x_1,\ldots,x_N), \tag{3}$$

$$\Phi_i^N = \sum_k B_{ik}\psi_k^N(x_1,\ldots,x_N), \tag{4}$$

where $A_{fk}^{(-)}(k_f)$ and B_{ik} are energy-dependent expansion coefficients determined from matching the wave functions (3) and (4) to the well-known asymptotic solutions of the system, and x_i stands for the space-spin coordinates of the ith electron. The R-matrix basis functions ψ_k^N in turn are written in the close-coupling form

$$\Psi_k^N(x_1,\ldots,x_N) = \mathcal{A}\sum_{ij} a_{ijk}\phi_i^{N-1}(x_1,\ldots,x_{N-1})\eta_{ij}(x_N) + \sum_p b_{kp}\chi_p^{(N)}(x_1,\ldots,x_N). \tag{5}$$

Here, η_{ij} are the continuum orbitals orthogonalized with respect to the target orbitals, and $\mathcal{A}$ is an antisymmetrization operator. Coefficients a_{ijk} and b_{kp} are variational parameters determined by the matrix diagonalization. The summation in the second term of Eq. (5) runs over configurations χ_p, where all electrons are placed in target-occupied and virtual molecular orbitals. The choice of appropriate χ_p is crucial. These are L^2 configurations and are needed to account for polarization and for correlation effects arising from excitations in the neutral molecule.

To calculate the photoionization of OH radicals with the UKRMOL+ package [14], we first construct the molecular orbitals that ensure a good description of both continuum and bound wave functions. Then we construct the target state wave functions with sufficient quality. Finally, we generate the continuum orbitals.

B. Target model

For the two electronic states of OH radicals that are investigated in the present work, the multichannel close-coupling calculations were performed at the corresponding equilibrium geometries, namely, $R_e = 0.9697$ Å for the $X\,^2\Pi$ ground state and $R_e = 1.0121$ Å for the $A\,^2\Sigma^+$ excited state [22]. The Hartree-Fock electronic configuration for the ground state of OH radicals is $1\sigma^2 2\sigma^2 3\sigma^2 1\pi^3$, and that for the first excited state is $1\sigma^2 2\sigma^2 3\sigma^1 1\pi^4$ [23]. The molecular orbitals were generated using the MOLPRO suite of programs [24] with the self-consistent field Hartree-Fock method. Three different basis sets including 6-31G**, 6-311G*, and 6-31 + G** were tested to obtain accurate target orbitals. The complete active space (CAS) CI method was used to deal with photoionization of the OH radical. In the CAS-CI model, four electrons in the inner molecule orbitals 1σ and 2σ are frozen, and the remaining five electrons are allowed to occupy freely all the other available molecule orbitals.

TABLE I. Vertical ionization potentials (in eV) for OH radicals obtained with 6-31G** (BS1), 6-311G* (BS2), and 6-31+G** (BS3) basis sets.

State	BS1	BS2	BS3	Expt.	Principal CSF
$X\,^3\Sigma^-$	12.80	12.83	12.87	13.01[a,b] 12.96[c]	$(1\pi)^{-1}$
$a\,^1\Delta$	15.10	15.13	15.18	15.17[a,b]	$(1\pi)^{-1}$
$b\,^1\Sigma^+$	16.79	16.84	16.89	16.61[a] 16.48[b]	$(1\pi)^{-1}$
$A\,^3\Pi$	16.82	16.86	16.86	16.48[a] 16.17[b]	$(3\sigma)^{-1}$
$c\,^1\Pi$	19.21	19.30	19.30	19.21[b]	$(3\sigma)^{-1}$
$d\,^1\Sigma^+$	24.67	24.77	24.75		$(3\sigma)^{-1}(1\pi)^{-1}(4\sigma)^{+1}$
$B\,^3\Pi$	29.89	29.64	29.87		$(1\pi)^{-2}(4\sigma)^{+1}$
$C\,^3\Sigma^-$	30.24	29.93	30.12		$(3\sigma)^{-1}(1\pi)^{-1}(4\sigma)^{+1}$
$e\,^1\Pi$	30.75	30.46	30.72		$(1\pi)^{-2}(4\sigma)^{+1}$
$D\,^3\Delta$	31.92	31.67	31.94		$(3\sigma)^{-1}(1\pi)^{-1}(4\sigma)^{+1}$

[a]From Ref. [6].
[b]From Ref. [8].
[c]From Ref. [7].

The calculated vertical ionization potential (IPs) for the first ten low-lying states are tabulated in Table I, together with the previous experimental results [6–8] for comparison. As shown in the table, both 6-31G** and 6-311G* basis sets predict very similar IPs. The values are in fair agreement with the experimental results [6–8], though ours are 0.2–0.7 eV higher. The 6-31 + G** basis set including the diffuse functions does not improve the IPs, but required the use of a larger R-matrix radius and thus more computational resources. To balance the computational cost and the quantity of the target description, we chose to use the 6-311G* basis set in the photoionization calculations.

In Table I, we give the orbital occupation differences between the HF neutral target wave function and the principal configuration state functions (CSFs) of the ion states. It is clearly evident that removal of a single electron gives rise to various states. Some of the configurations have the same primary configuration and differ by their spin symmetry. We observe that the triplet states lie energetically lower than the singlet states in agreement with Hund's rule.

C. Inner and outer regions

In the inner region, the continuum orbital is commonly constructed from GTOs centered on the center of mass of the system. GTOs are not suitable to represent the highly oscillating behavior of the true continuum functions both over an extended radical range and when higher values of the photon energy need to be considered. Therefore the size of R-matrix spheres is limited and the collision energies that can be treated are restricted. The suitable base for this task is to use B-spline functions. In the present work, both types of continuum bases (GTO and BTO) are tested. The orthogonalization deletion threshold for GTOs is 10^{-9} and that for BTOs is 10^{-5}. The value of the R-matrix radius taken to enclose the total charge of the target inside the inner region was $15a_0$. The maximum angular momenta $l_{\max} = 4$ and 5 were used to check the convergence of partial wave expansion. In BTO calculations, the B splines of order 6 are employed, and the number of radical B splines in the basis is 20. The first two radical B splines are not included in the basis due to them having a nonzero first derivative at the starting point.

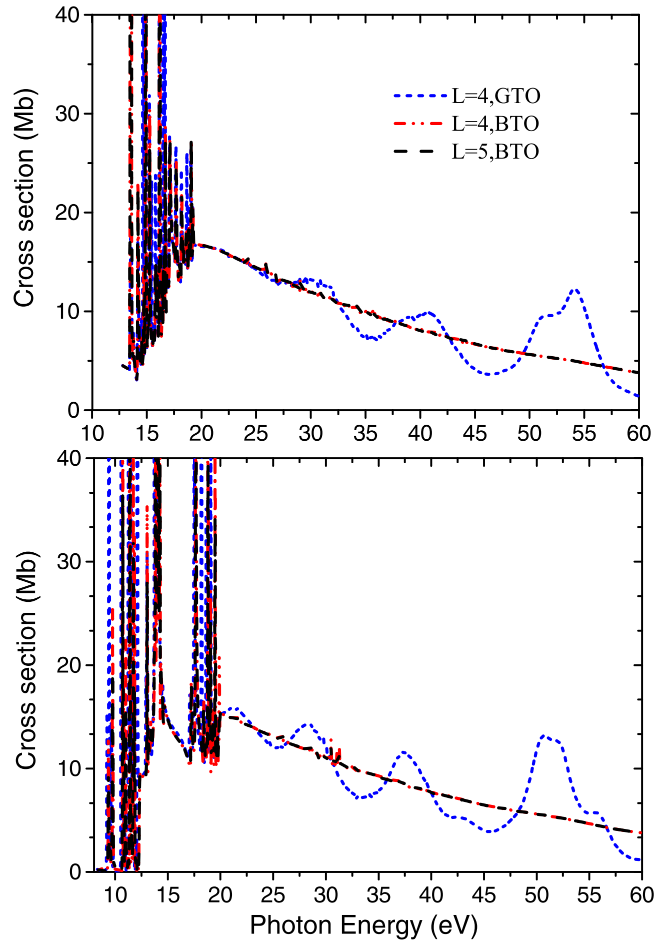

FIG. 1. Total photoionization cross sections calculated with GTO and BTO and different partial waves for $l = 4$ and 5, from the $X\,^2\Pi$ ground state (upper panel) and the first excited state $A\,^2\Sigma^+$ (lower panel) of OH radicals.

In the present calculations, the L^2 configurations in Eq. (5) can be written in two classes, $(\text{core})^4(\text{CAS})^4(\text{virtual})^1$ and $(\text{core})^4(\text{CAS})^5$. Here the active space is composed of 3σ-10σ, 1π-4π, and 1δ orbitals. The inclusion of a large number of target states was necessary to converge the close-coupling expansion and to avoid any unphysical pseudoresonances that may otherwise appear at higher energies related to target states left out of the expansion. The different numbers of the target states were included in the close-coupling calculations to test the convergence of the close-coupling expansion.

III. TESTS OF MODELS

Our total photoionization cross sections from the ground state and the first excited state of OH radicals with GTO for partial waves up to $l = 4$ and BTO for $l = 4$ and 5, are presented in the upper and lower panels of Fig. 1. As shown in the picture, the total cross sections with BTO base show the negligible differences between the partial waves up to $l = 4$ and $l = 5$. This indicates that $l_{\max} = 4$ is sufficient to obtain converged photoionization results for OH in the present calculations.

Both GTO and BTO produce almost the same results in the low-energy region below 25 eV for photoionization from the ground state and below 20 eV for photoionization from the first excited state. While at the higher photon energy, the cross sections for GTO basis begin to oscillate along the cross section for the BTO basis, indicating the GTO basis may be not good enough to describe the continuum states. Indeed, standard GTO basis functions are characterized by their exponential decrease that does not make them suitable to describe the oscillatory behavior of the continuum wave function up to large distances from the parent ion. Recent studies, performed by Ruberti *et al.* [25] using the highly correlated algebraic diagrammatic construction and by Cukras *et al.* [26] using linear response coupled cluster methods for electronic excitations in conjunction with the Stieltjes imaging technique, indicated that the use of GTOs in molecular photoionization cross-section calculations leads to the onset of major inaccuracies in the calculated cross sections at about 70 eV above ionization threshold. Moreover, these studies showed that even very careful GTO selections cannot afford high-energy features and high resolution. In contrast, BTO basis functions are very flexible and accurately describe both the bound and continuum states with minimal numerical dependencies, and are becoming popular for continuum calculations [27]. We expect the present BTO results are reliable. Figure 1 shows our cross section for the BTO basis.

Figure 2 illustrates the effect of including more target states in the CC expansion. Three models including 9, 40, and 80 target states are used in the CC expansion for photoionization from the ground state and the first excited state. Of the nine target states three states are in $^1A_1$ symmetry, and each one is in $^1B_1$, $^1B_2$, $^1A_2$, $^3B_1$, $^3B_2$, and $^3A_2$ symmetries. These target states correspond to the first six states in Table I in the $C_{\infty V}$ point group. For the 40 target states CC model, the calculation includes each 5 target states in every singlet and triplet symmetry and for the 80 target states model it includes each 10 target states in eight symmetries. For photoionization from the ground state, total cross sections in the 40 states CC model and the 80 states CC model are slightly lower than that in the 9 states CC model. But for photoionization from the first excited state, the cross sections calculated with 40 states and 80 states are much bigger. In order to clarify these large differences, we also perform the 14 states CC calculations for the photoionization from the first excited state. Here the 14 target states in the C_{2V} point group correspond to the first 9 states in Table I. As shown in Fig. 2, clearly, with increasing the target states to 14 states in the CC calculation, the total cross section increases and shows smaller difference when comparing with 80 states CC results. The retention of a large number of electronic channels in the CC model provides the necessary polarization potential in an *ab initio* way, which is crucial for determining the cross section. The great similarity of the curves corresponding to the 40 states and the 80 states CC models provides an indication that a good convergence with respect to multichannel coupling has been achieved to

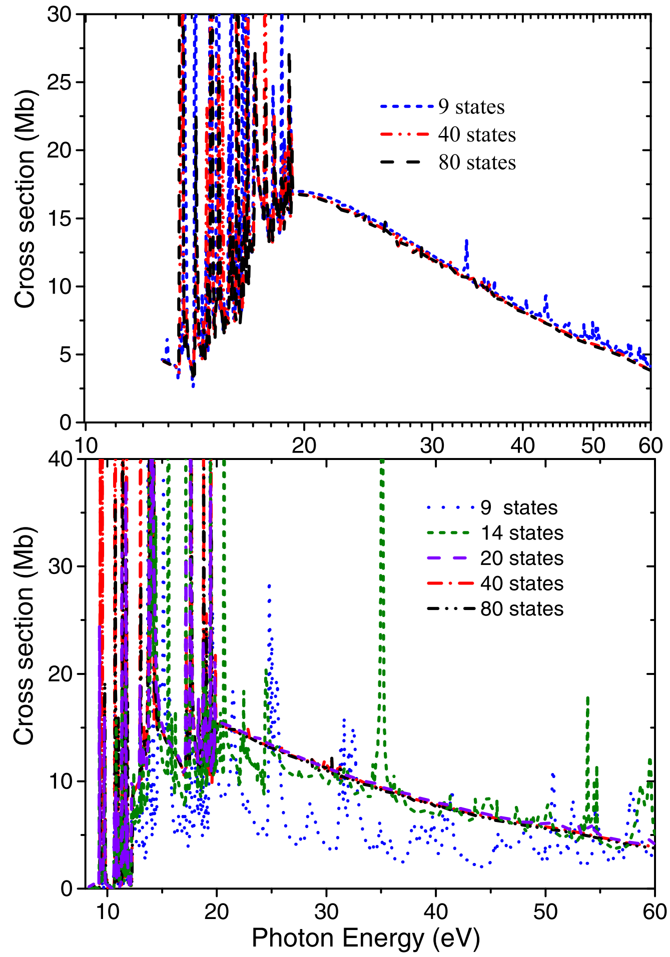

FIG. 2. Total photoionization cross sections calculated with three different models: 9 states, 40 states, and 80 states CC calculations from the $X\,^2\Pi$ ground state (upper panel) and the first excited state $A\,^2\Sigma^+$ (lower panel) of OH radicals.

the photoionization from the ground state and the first excited state of OH radical. Much sharper peaks are observed at higher energies in 9 states CC cross sections from the first excited state, which might be pseudoresonances. This reveals that multichannel coupling effects on the cross section are more important for ionization from the excited state than from the ground state.

As shown above, the CC model including 80 target states with the BTO continuum and angular momentum up to $l = 5$ is our best model to describe the photoionization of OH radical. And then we will discuss the results from this model in the following section.

IV. RESULTS AND DISCUSSIONS

The total photoionization cross sections from the $X\,^2\Pi$ ground state of OH radicals in the energy region 13–15.1 eV are shown in Fig. 3(a), with the available experimental results for comparison. In general, our results are a little higher than the cross sections measured by Dodson *et al.* [9] from the threshold to 14.21 eV, but slightly lower than the measurements of Harper *et al.* [10] in the energy region 13–15.1 eV except for the resonant region. The relative photoionization

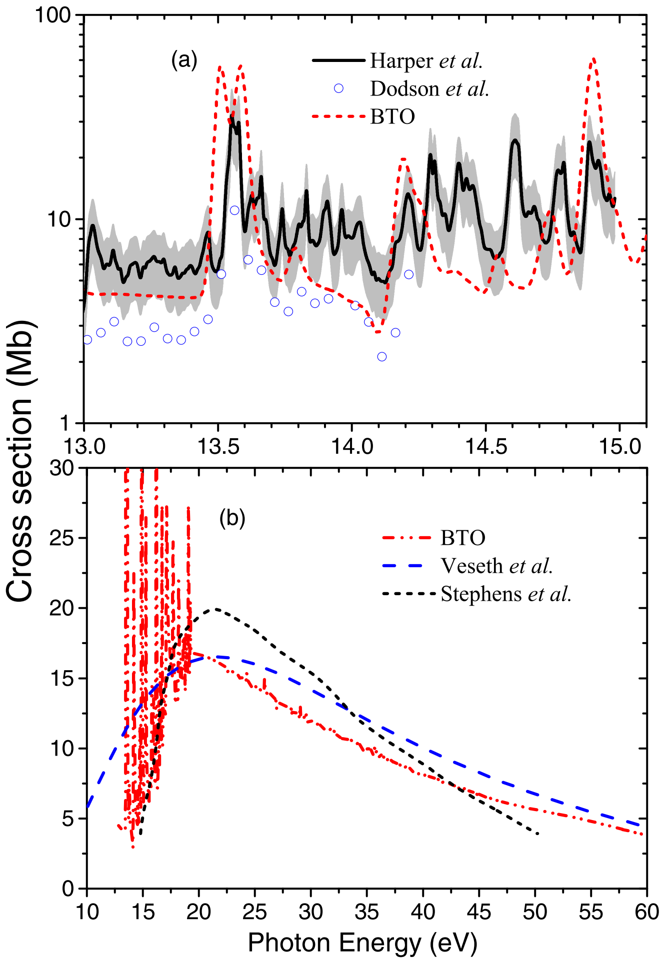

FIG. 3. Total photoionization cross sections from the $X\,^2\Pi$ ground state of OH radicals calculated with our best model in the energy range (a) 13–15.1 eV (the gray-shaded area defines the 2σ uncertainties) and (b) 10–60 eV. Comparison with the available results.

spectra of OH radicals measured by Dehmer *et al.* [7] and Culter *et al.* [8] have a similar shape to the results of Harper *et al.* [10], and are not discussed in the present paper.

As shown in Fig. 3(a), our calculations predict several resonancelike features in the total photoionization cross section. In addition to the minimum at 14.1 eV, there are three peaks around 13.55, 13.79, and 14.19 eV, which are in good agreement with the experimental results of Dodson *et al*. [9] as well as Harper *et al.* [10]. We used a fine mesh for photon energies in steps of 0.04 eV to scan and properly separate the possible resonance structures. The first broad autoionization peak splits into two subpeaks centered at 13.51 and 13.59 eV, which agrees well with the higher-resolution spectra of Harper *et al.* [10]. The resonances in multichannel scattering are characterized not only by the corresponding structures in the cross sections but also—more important for their analysis—by the sudden jump of the eigenphase sum by π radians over a relatively narrow energy range. By analyzing the eigenphase sums, the first subpeak located at 13.51 eV is from the A_1 and A_2 symmetries and the second subpeak at 13.59 eV is from the B_2 symmetry. Both are termed as shape resonances. The peaks at 13.79 and 14.19 eV belong to shape resonances with B_2 and A_2 symmetries, respectively. At higher photon energies, the present cross sections also show several prominent peaks, supporting the work of Harper *et al.* [10].

In Fig. 3(b) the present total photoionization cross sections are compared with the previous theoretical results of Stephen *et al.* [11] obtained by using MSHF potentials and numerical photoelectron continuum orbitals and Veseth *et al.* [12] obtained with the many-body perturbation theory in the energy region between 10 and 60 eV. All the theoretical profiles show a common behavior: the cross sections increase at threshold until reaching their maximum, and then gradually decrease at the higher excited energy. Strong electron correlation including in the present calculations causes two dramatic changes in the total cross section, as can be seen by comparing the MSHF profile with our multichannel results. On the one hand, the cross-sectional maximum shifts toward the threshold. The maximum in the cross section of 21.0 Mb at about 21.4 eV of photon energy computed at the MSHF level drops to 16.8 Mb at about 19.5 eV in our multichannel results. On the other hand, the MSHF results display larger cross sections in the energy region from 20 to 42 eV, but become smaller at the higher photon energies between 42 and 50 eV. The theoretical results obtained by Veseth *et al.* [12] are a little higher than our results at the photon energy beyond 22 eV. Dodson *et al.* [9] and Harper *et al.* [10] have noted that the calculated cross sections of Veseth *et al.* contain the nonionization processes, which leads to a larger cross section in their calculations.

Figure 4 presents the partial cross section and asymmetry parameter for photoionization from the ground state of OH leading to the $X\,^3\Sigma^-$ state of OH^+ ions. A comparison is made between our results and the theoretical work of Stephen *et al.* [11] and Riahi *et al.* [13]. Up to 20 eV, the present cross sections are consistent with the theoretical cross section of Stephen *et al.* and Riahi *et al.* In the energy range 20–40 eV, our result is consistently below the other theoretical ones. In the energy range 40–50 eV, the differences between them become very small. A comparison between our results and the calculations of Stephen *et al.* [11] suggests the inclusion of the correlation effects cause a shift of the MSHF profile toward threshold together with a loss of intensity in the overall process. Similar to the calculated cross section, our asymmetry parameter has numerous sharp peaks, while the MSHF asymmetry parameter is very smooth. In the energy region 20–50 eV, our asymmetry parameter is sizably larger than the MSHF asymmetry parameter. With respect to the behavior of the cross section, the asymmetry parameter is seen to be more affected by electron correlation effects, as can be judged from the overall large differences between our results and the calculations of Stephen *et al.* Above 50 eV, there are no available theoretical or experimental data for comparison. For the purpose of clarifying these differences, an extra calculation is also carried out with the larger basis set 6-311G**. The obtained cross sections and asymmetry parameters show almost the same shape as with the results with the 6-311G* basis set. This means the differences from the basis sets can be ruled out.

Figures 5 and 6 show cross sections and asymmetry parameters for ionization from the ground state of OH leading to the $a\,^1\Delta$ and $b\,^1\Sigma^+$ states of OH^+ ions, respectively, with the previous theoretical results of Stephen *et al.* [11]. Compared with

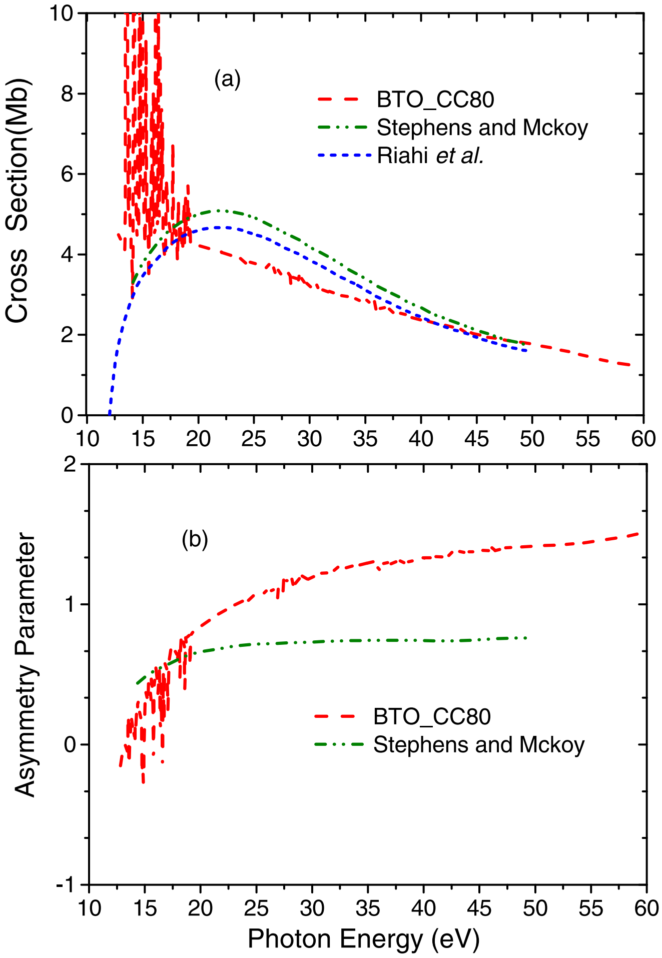

FIG. 4. Photoionization cross section and asymmetry parameter for ionization from the ground state of OH leading to the $X\,^3\Sigma^-$ state of OH^+ ions.

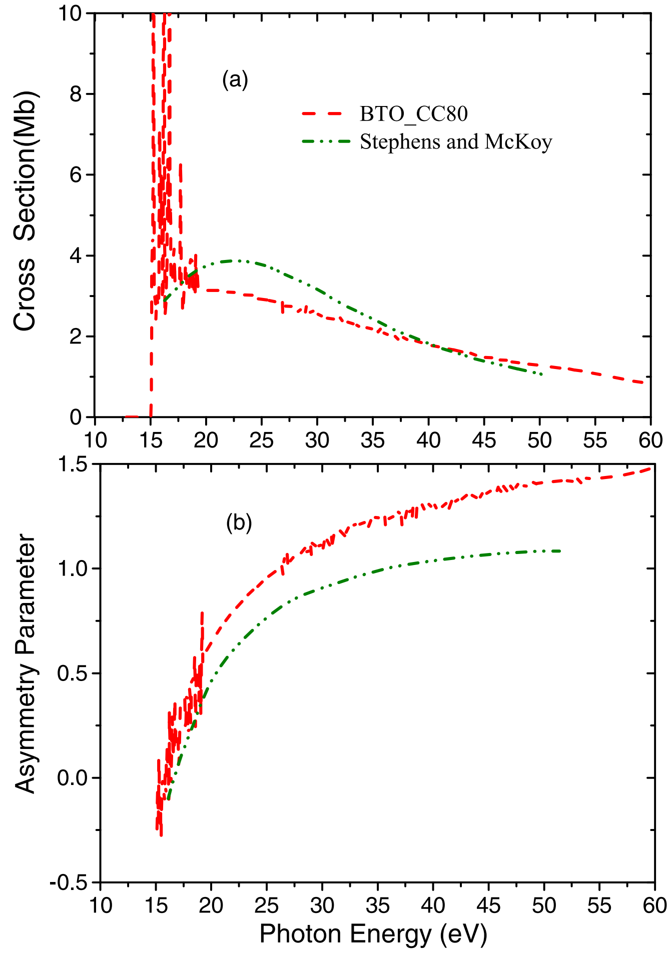

FIG. 5. Photoionization cross section and asymmetry parameter for ionization from the ground state of OH leading to the $a\,^1\Delta$ state of OH^+ ions.

the results of Stephen *et al.*, our photoionization observables leading to the $a\,^1\Delta$ state of OH^+ ions show a consistent trend as those to the $X\,^3\Sigma^-$ state. In the case of photoionization leading to the $b\,^1\Sigma^+$ state of OH^+ ions, both cross sections show a resonant behavior with maxima centered at about the same photon energy 22.7 eV. In the energy region below 40 eV, our cross sections are lower. But with the photon energy beyond 40 eV it is reversed and the present results are a bit higher. As shown in Fig. 6(b), both the asymmetry parameters show the monotonic increase to a limited value of 1.3, the MSHF profile lying consistently above our multichannel results.

Now we compare the calculated partial cross section with the experimental data. The He Iα photoelectron spectroscopy of OH radicals has been measured by van Lonkhuyzen and de Lange [6]. They obtain the relative intensities of $X\,^3\Sigma^-$, $a\,^1\Delta$, and $b\,^1\Sigma^+$ states of OH^+ ions to be 2.9 ± 0.2, 1.6 ± 0.2, and 1.0 ± 0.2, respectively, at a photon energy of 21.2 eV. At this photon energy, our $X\,^3\Sigma^-/b\,^1\Sigma^+$, and $a\,^1\Delta/b\,^1\Sigma^+$ branching ratios are 2.8 and 2.1, respectively, in reasonable agreement with the experimental values when taking the combined errors of the relative intensities into account.

Finally, Fig. 7 depicts photoionization cross sections and asymmetry parameters for ionization from the $A\,^2\Sigma^+$ excited state of OH leading to the $A\,^3\Pi$, $B\,^3\Pi$, and $C\,^3\Sigma^-$ states of OH^+ ions. The magnitude of cross section for the A state decreases slowly from 15 Mb above the threshold to 2 MB at an energy of 60 eV. The cross section for the B and C states are relatively flat above threshold and are similar to each other. The same trend is observed for B and C states, where both magnitudes change from about 3 Mb near the threshold to 1 MB at an energy of 60 eV. The asymmetry parameters for both A and B states have remarkably similar shapes and magnitudes, starting from -0.5 near the thresholds and increasing monotonically to 1.5 around 60 eV. For the C state, the asymmetry parameter decreases rapidly near the threshold and then increases slowly to 1 at an energy of 60 eV.

V. SUMMARY

We performed a detailed study of photoionization of the ground and first excited state of OH radicals, and presented results for the total as well as partial cross sections and asymmetry parameters. The calculations were performed with the multichannel *R*-matrix method with configuration interaction. With the CAS-CI model using the 6-311G* basis set, the GTO continuum basis provides a similar quality of description as

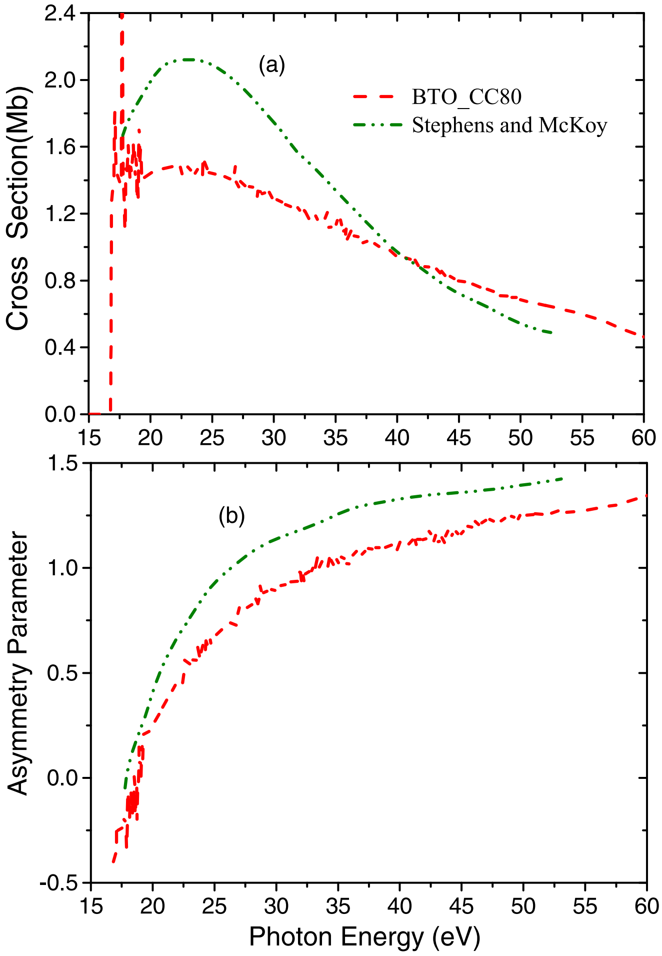

FIG. 6. Photoionization cross section and asymmetry parameter for ionization from the ground state of OH leading to the $b\,^1\Sigma^+$ state of OH^+ ions.

the BTO base up to 25 eV for ground state, and up to 20 eV for first excited state. While at higher energy region, oscillatory behavior appearing in the cross section of GTO basis indicates it may be not stable. A comparison of the total cross section from the ground and first excited states in the partial waves between $l_{\max} = 4$ and 5 shows the convergence for partial waves $l_{\max} = 4$. The importance of including the correlation effects has been revealed by comparing with existing theoretical calculations based on the MSHF method.

Inclusion of more states in the CC expansion has small effects on the total cross section for ground state. While the study of photoionization from the first excited state of OH radicals has revealed the presence of strong multichannel coupling effects, which dramatically affects the cross sections when compared to the 9 states CC results.

Experimental measurements of the photoionization dynamical parameters, such as partial cross sections and asymmetry parameters, are needed in order to test and verify the role played by the various types of many-bady effects in the photoeffect of such a molecular system. But they are challenging, in particular, for free radicals and therefore are often missing or are found in the literature within a wide range. We provide higher level calculations of the cross section, as well as for calculations that include resonant excitation processes. And our calculations enlighten the disagreement between the two different experimental approaches. We hope that the dearth of data on the photon and OH radicals scattering system encourages further experimental and theoretical investigations. Such data sets are needed in a variety of applications from aeronomy to plasma modeling.

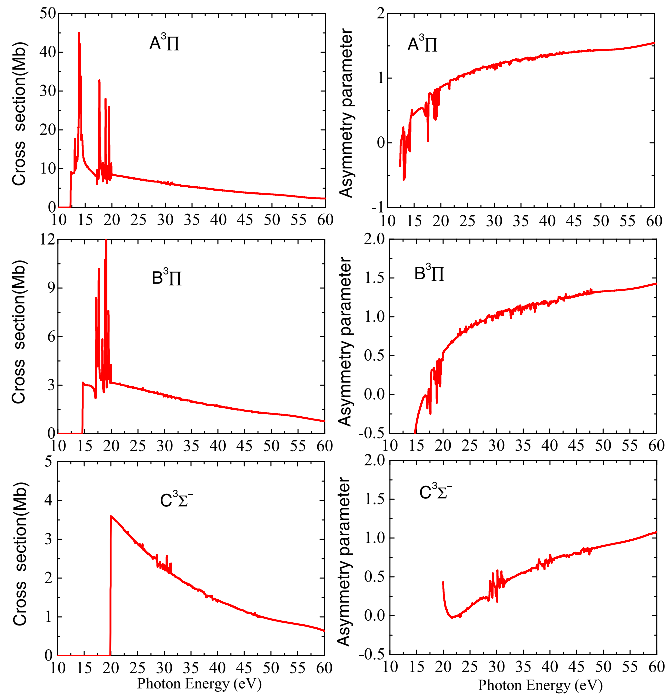

FIG. 7. Photoionization cross section and asymmetry parameter for ionization from the $A\,^2\Sigma^+$ excited state of OH leading to the $A\,^3\Pi$, $B\,^3\Pi$, and $C\,^3\Sigma^-$ states of OH^+ ions.

ACKNOWLEDGMENTS

This work was supported by the Natural Science Foundation of China under Grants No. U1504109 and No. 11604085, and of Henan Province under Grant No. 212300410054, the Program for Science and Technology Innovation Talents in the Universities of Henan Province under Grant No. 19HASTIT018, and the Science Foundation of Henan Normal University under Grants No. YQ201601 and NO. 2021PL14.

[1] J. W. Gallagher, C. E. Brion, J. A. R. Samson, and P. W. Langhoff, J. Phys. Chem. Ref. Data **17**, 9 (1988).
[2] P. Croteau, J. B. Randazzo, O. Kostko, M. Ahmed, M. C. Liang, Y. L. Yung, and K. A. Boering, Astrophys. J. **728**, L32 (2011).

[3] B. J. Finlayson-Pitts and J. N. Pitts, Jr., *Chemistry of the Upper and Lower Atmosphere: Theory, Experiments, and Applications* (Academic, New York, 1999).
[4] J. A. Miller, M. J. Pilling, and J. Troe, Proc. Combust. Inst. **30**, 43 (2005).
[5] S. Weinreb, A. H. Barrett, M. L. Meeks, and J. C. Henry, Nature (London) **200**, 829 (1963).
[6] H. van Lonkhuyzen and C. A. de Lange, Mol. Phys. **51**, 551 (1984).
[7] P. Dehmer, Chem. Phys. Lett. **110**, 79 (1984).
[8] J. N. Cutler, Z. X. He, and J. A. R. Samson, J. Phys. B: At., Mol. Opt. Phys. **28**, 4577 (1995).
[9] L. G. Dodson, J. D. Savee, S. Gozem, L. Shen, A. I. Krylov, C. A. Taatjes, D. L. Osborn, and M. Okumura, J. Chem. Phys. **148**, 184302 (2018).
[10] O. J. Harper, M. Hassenfratz, J.-C. Loison, G. A. Garcia, N. de Oliveira, H. R. Hrodmarsson, S. T. Pratt, S. Boyé-Péronne, and B. Gans, J. Chem. Phys. **150**, 141103 (2019).
[11] J. A. Stephens and V. McKoy, J. Chem. Phys. **88**, 1737 (1988).
[12] L. Veseth and H. P. Kelly, Phys. Rev. A. **45**, 4621 (1992).
[13] R. Riahi, P. Teulet, Y. Cressault, A. Gleizes, and Z. Ben Lakhdar, Eur. Phys. J. D **49**, 185 (2008).
[14] Z. Mašín, J. Benda, J. D. Gorfinkiel, A. G. Harvey, and J. Tennyson, Comput. Phys. Commun. **249**, 107092 (2020).
[15] D. S. Brambila, A. G. Harvey, K. Houfek, Z. Mašín, and O. Smirnova, Phys. Chem. Chem. Phys. **19**, 19673 (2017).
[16] P. Modak and B. Antony, Astrophys. J. **887**, 262 (2019).
[17] P. Modak and B. Antony, J. Phys. B: At., Mol. Opt. Phys. **53**, 045202 (2020).
[18] J. Benda, J. D. Gorfinkiel, Z. Mašín, G. S. J. Armstrong, A. C. Brown, D. D. A. Clarke, H. W. van der Hart, and J. Wragg, Phys. Rev. A. **102**, 052826 (2020).
[19] J. Tennyson, C. J. Noble, and P. G. Burke, Int. J. Quantum Chem. **29**, 1033 (1986).
[20] A. G. Harvey, D. S. Brambila, F. Morales, and O. Smirnova, J. Phys. B. **47**, 215005 (2014).
[21] P. G. Burke, *R-Matrix Theory of Atomic Collisions* (Springer-Verlag, Berlin, Heidelberg, 2011).
[22] K. P. Huber and G. Herzberg, *Constants of Diatomic Molecules* (Van Nostrand, New York, 1979).
[23] E. F. van Dishoeck and A. Dalgarno, J. Chem. Phys. **79**, 873 (1983).
[24] H.-J. Werner, P. J. Knowles, G. Knizia, F. R. Manby, and M. Schütz, WIREs Comput. Mol. Sci. **2**, 242 (2012).
[25] M. Ruberti, R. Yun, K. Gokhberg, S. Kopelke, L. S. Cederbaum, F. Tarantelli, and V. Averbukh, J. Chem. Phys. **139**, 144107 (2013).
[26] J. Cukras, S. Coriani, P. Decleva, O. Christiansen, and P. Norman, J. Chem. Phys. **139**, 094103 (2013).
[27] T. Moitra, A. Ponzi, H. Koch, S. Coriani, and P. Decleva, J. Phys. Chem. Lett. **11**, 5330 (2020).